1

Structure and Physical Properties of Metal Halide Perovskites

1.1 Crystal Structure of Perovskite Materials

Since their discovery by Gustav Rose in 1839, perovskite materials have enjoyed a lengthy and fascinating history. Over the decades, a wide variety of perovskite materials have found uses in numerous applications, spanning from piezoelectric and optoelectronic devices to ferroelectric materials, superconductors, magnetoresistive sensors, catalysts, and ionic conductors, among others [1–7]. Halide perovskites, a specific category, have been the subject of extensive research for more than half a century [8]. As depicted in Figure 1.1, the general formula for perovskites is typically ABX_3, where A represents a monovalent cation (such as $CH_3NH_3^+$ (MA^+), $NH_2CHNH_2^+$ (FA^+), or Cs^+), B denotes a metal cation (generally Pb^{2+} or Sn^{2+}), and X represents a halogen anion (generally Cl^-, Br^-, or I^-).

Metal halide perovskite garnered significant attention from the scientific community following its application as a photosensitive layer in a dye-sensitized solar cell (DSSC) in 2009. Since then, comprehensive research has delved into its remarkable optical and electronic properties, marking it as an extremely promising material for diverse applications [10, 11].

Perovskite materials possess excellent physical properties, such as low defect density, high carrier mobility, long charge carrier lifetime, and long electron–hole diffusion length [12–15]. Therefore, perovskite-based solar cells have shown high defect tolerance, enabling them to achieve good photovoltaic performance even at relatively low purity levels of up to 90% [11, 16]. In addition, metal halide perovskites are not only used as a light-absorbing layer in solar cells but also widely utilized in the light-emitting layer of light-emitting diodes (LEDs) [11, 17–19]. Compared to conventional light-emitting materials, metal halide perovskites have unique optical properties such as tunable bandgap, high color purity, wide color gamut, and high fluorescence quantum efficiency [20–22]. Additionally, perovskite materials can be prepared as bulk single crystals, microcrystals, or nanocrystals (NCs) using a simple and cost-effective solution-based method [23].

Perovskite Light Emitting Diodes: Materials and Devices, First Edition. Hong Meng.

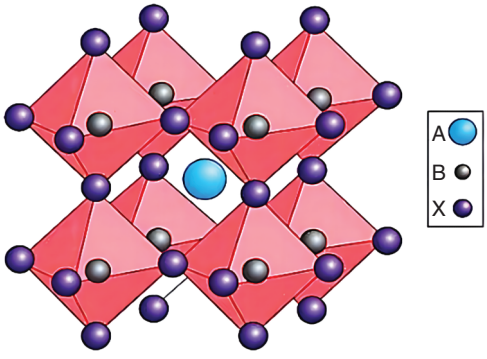

Figure 1.1 Crystal structure of perovskite. Source: Quan et al. [9]/ John Wiley & Sons.

1.2 Exciton Effects in Perovskite Materials

1.2.1 Definition of an Exciton

When a semiconductor absorbs a photon with energy greater than or equal to its bandgap energy, the electron is excited from the valence band to the conduction band, leaving behind a hole in the valence band. The electron and hole are attracted to each other due to the Coulomb force, forming an electron–hole pair, which is also known as an exciton. The distance between the electron and the hole is called the exciton Bohr radius, and its value depends on the material, typically ranging from 2 to 50 nm [24]. Excitons have different radii based on their size, which are divided into two types: free excitons (Wannier excitons) and bound excitons (Frenkel excitons) [25], as shown in Figure 1.2.

The prevalence of free excitons in most perovskite materials can be explained by the conventional hydrogen atom model, which is mainly dependent on the effective masses of electrons and holes in the semiconductor. The energy levels of excitons

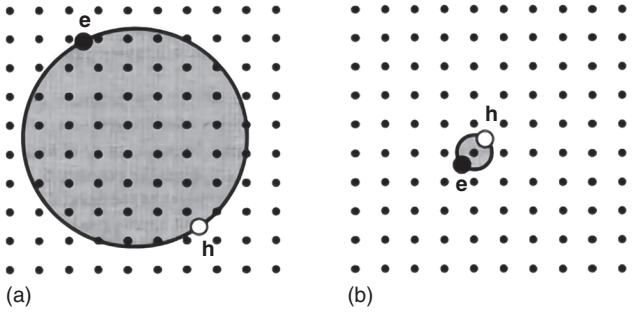

Figure 1.2 (a) Free exciton; (b) bound exciton. Source: Adapted from Dresselhaus [25].

can be expressed by Eq. (1.1).

$$E_n = E_g - \frac{R^*}{n^2} \tag{1.1}$$

where E_g is the forbidden band width and R^* is the effective Rydberg constant of the exciton.

In semiconductors, the effective mass of carriers is typically smaller than that of excitons, resulting in the screening of carriers by the lattice. This leads to the effective Rydberg constant being expressed as the normalized Rydberg constant (Eq. 1.2).

$$R^* = R_0 \mu / m_0 \varepsilon_r^2 \tag{1.2}$$

When the mass of the exciton is reduced to $1/\mu = 1/m_h + 1/m_e$ (m_h, m_e are the effective masses of holes and electrons, respectively, and ε_r is the relative permittivity of the crystal), it mainly originates from carriers that are screened by the lattice. As a result, the exciton binding energy R^* depends on the effective mass of the carriers and the dielectric constant of the crystal. Numerous studies have shown that the dielectric constants of perovskites can be very different in the static case and when photoinduced, in the case of halogenated perovskites, the dielectric constant is about $\varepsilon_s \approx 30$ at rest, whereas under high-frequency light irradiation, its dielectric constant $\varepsilon_\infty \approx 30$. Consequently, the calculation of the exciton binding energy of perovskites varies considerably between reports.

1.2.2 Self-Trapping Excitons in Perovskite Materials

Self-trapping excitons in perovskite materials are essential for the study of luminescent materials, particularly for white perovskite materials. In soft lattices, the lattice couples to carriers, causing electroelastic distortions and reducing the lattice's symmetry. These distortions create chiral carriers, also known as polaritons, which can be categorized into large and small polaritons based on their potential well depth and size [26]. Large polaritons exhibit a strong long-range Coulomb interaction and can be delocalized over several cells. Small polaritons, on the other hand, emerge from the short-range distortion of the lattice caused by localized carriers. Self-trapped excitons resemble small polaritons as their Bohr radius is small and closely linked to the lattice distortion (Figure 1.3).

The intrinsic self-trapped exciton is different from a permanent defect in the material [28], which can be imagined as a hard ball (electron/hole/exciton) falling onto a soft rubber sheet (distorted lattice); the ball falls into a potential well of its own formation, and the sheet distorts mainly from the appearance of the ball. After the ball leaves, the sheet returns to its original shape (Figure 1.4a). When there is already an indentation (permanent defect) in the sheet, it is also possible for the ball to fall into this indentation (Figure 1.4b). However, when the ball interacts with an indentation in its vicinity, a new defect is formed, and the ball will fall into a new depth, which is called an exotic excitation (Figure 1.4c).

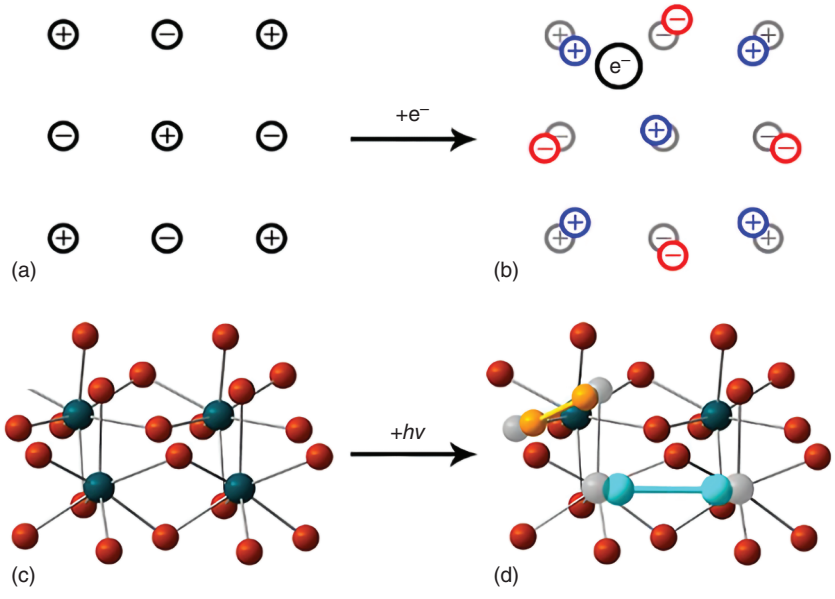

Figure 1.3 (a) and (b) Schematic diagram of the formation of a large polariton resulting from the addition of an electron to the ionic lattice, causing a long-range distortion of the lattice; (c) $PbBr_2$ crystal structure unit, with green and brown representing Pb and Br atoms, respectively; (d) self-trapped holes and self-trapped electrons formed by the orange Br_2^- and blue–green Pb_2^{3+} dimer, followed by the formation of photoexcitation. Source: Smith and Karunadasa [27]/American Chemical Society.

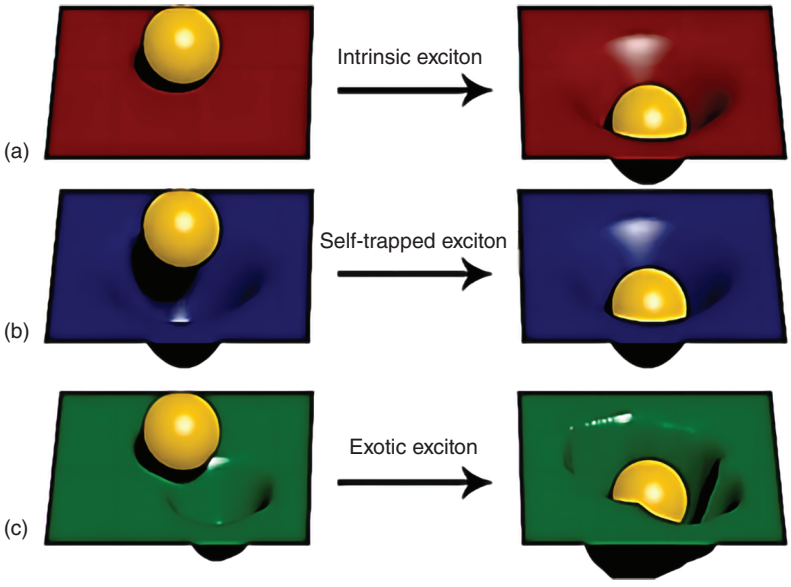

Figure 1.4 (a) Intrinsic exciton; (b) self-trapped exciton caught in a permanent trap; (c) exotic exciton (self-trapped exciton and permanent defect) interactions (in the figure, the ball represents the exciton and the rubber sheet represents the lattice). Source: Smith and Karunadasa [27]/American Chemical Society.

1.3 Size Effect of Perovskite Materials

For semiconductor nanocrystals that are extremely small or of zero size, the behavior of the exciton wave function – essentially, the behavior of electrons and holes – will be influenced by the limited space of the domain. As the size decreases, alterations occur in the density of the electronic states. Most notably, the forbidden band width increases, and the highest point of the valence band and the lowest point of the conduction band display discrete splitting energy levels. This is known as the quantum confinement effect [29]. As shown in Figure 1.5, as the size decreases, the bandgap of the semiconductor increases, resulting in a blueshift of the luminescence peak. Moreover, more discrete energy levels are generated, and the width of these discrete levels also increases.

The quantum confinement effect allows for tuning of the absorption and emission spectra by altering the size of particles while keeping the material components constant. Additionally, the scale of the quantum confinement domain varies in different directions due to variations in size and morphology, as shown in Figure 1.6 [31–33]. The size and shape of semiconductor nanocrystals greatly influence their optical and electrical properties, as changes in dimensionality can affect the bandgap and electrical conductivity of the material system. The confinement of

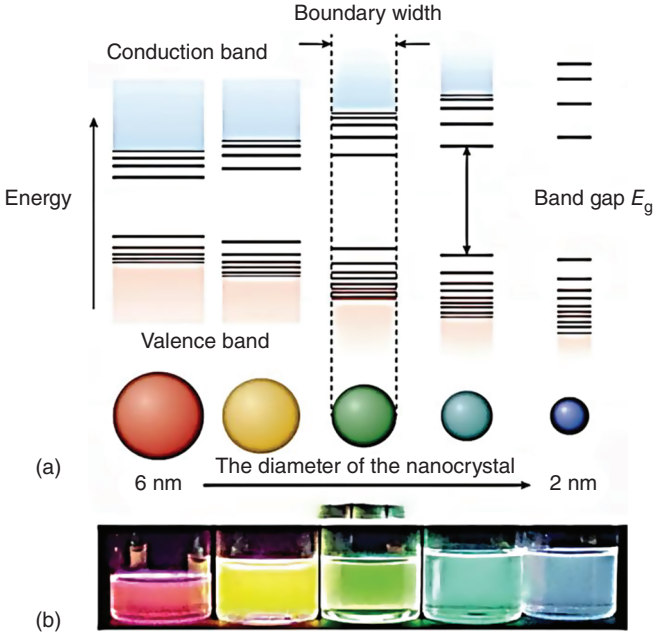

Figure 1.5 (a) Model of the quantum confinement effect: from this, it can be seen that as the bandgap of the semiconductor decreases in size, more discrete energy levels appear at the band edges, and the discrete width of the band edge energy levels increases further; (b) In the luminescence of five different sizes of CdSe quantum dot colloids under UV lamp irradiation, it can be seen that the luminescence changes from red to blue as the size changes from 6 nm to 2 nm. Source: Efros et al. [30], ©1996/Reproduced from American Physical Society.

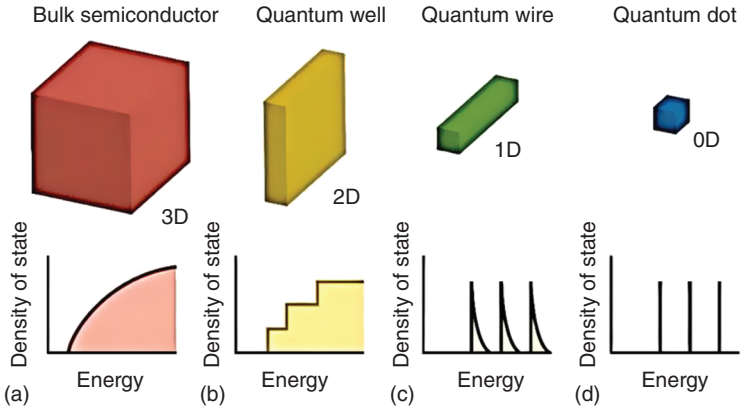

Figure 1.6 (a) Schematic diagram of the energy level structure of a semiconductor bulk; (b)–(d) semiconductor nanostructures of decreasing dimensionality (2D–1D–0D) and their electronic density of states. Source: Adapted from Efros et al. [30].

excitons in different directions results in the formation of zero-dimensional quantum dots, one-dimensional quantum lines, and two-dimensional quantum wells. As the quantum effect decreases, the growth of the material tends toward forming a three-dimensional bulk structure. In the quantum-constrained region, the exciton's fine structure becomes significant. This term refers to the division of exciton energy states due to the crystal's symmetry, anisotropy, and the exchange between electrons and holes. While the energy level splitting of excitons in nanocrystals is typically minor – usually on the scale of a few milli-electronvolts (meV), it can still influence the exciton's lifetime under different conditions. These conditions could include varying temperature fields and magnetic fields [31–39].

Phonons in semiconductors play a crucial role in determining their optoelectronic properties, as they are coupled to charge carriers and excitons. In semiconductor nanocrystals, the coupling between phonons and excitons differs from that in bulk materials due to the effects of dimensionality and quantum confinement (e.g. the phonon wavelength may be larger than the size of the nanocrystal). This coupling can lead to new energy pathways, affecting processes such as exciton dynamics, carrier cooling, and thermal transfer. The interaction with acoustic phonons results in the broadening of the optical transition linewidth, while coupling with optical phonons can induce chiral selection at low temperatures, thereby influencing phonon-assisted transitions.

In terms of device applications, metal halide perovskites meet the charge-transport and charge-injection requirements, with high diffusion lengths and optimum interface formation with most employed contacts. In the case of perovskite light-emitting diodes (PeLEDs), the emitter layer can consist of 3D, layered, or nanostructured perovskites, which are sandwiched between electron- and hole-transport layers and injection contacts [40] (Figure 1.7).

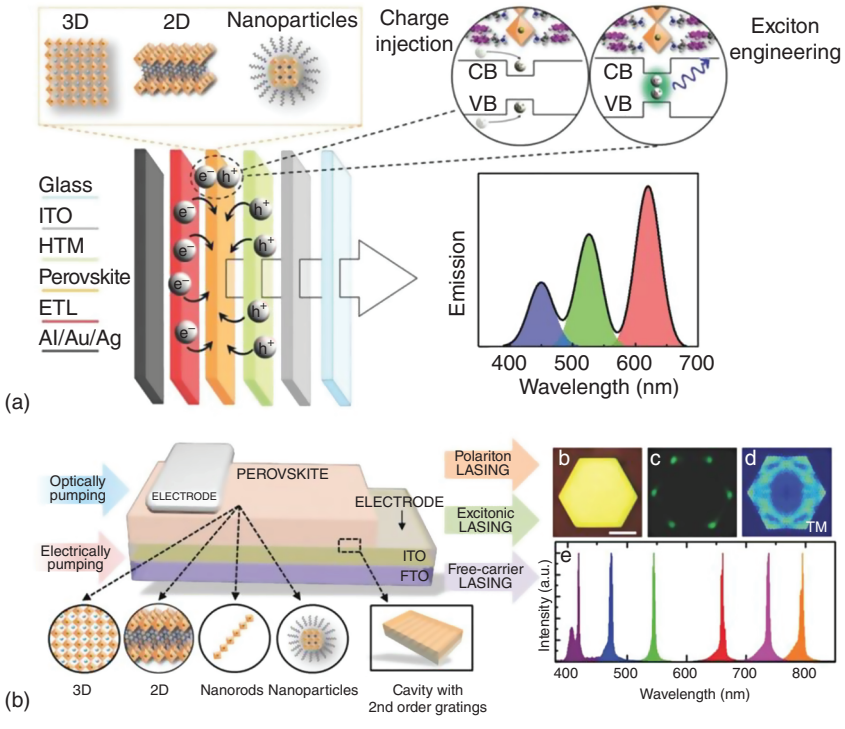

Figure 1.7 (a) Schematic representation of a PeLED device concept; (b) a perovskite laser device concept. Source: Veldhuis et al. [40]/Reproduced from John Wiley & Sons, Inc.

1.4 Luminescence Properties of Perovskite Materials

PeLEDs are experiencing rapid development and hold immense potential for various applications. As depicted in Figure 1.8, they are particularly notable in the visible region for applications such as display devices, high-brightness applications (e.g. projection displays and solid-state lighting), and augmented/virtual reality (AR/VR). With the shift in display technology from liquid crystal displays (LCDs) to active matrix organic light-emitting diodes (AMOLEDs), PeLEDs offer significant advantages due to their mild processing conditions and the possibility of direct integration onto thin-film transistor (TFT) backplanes. Furthermore, PeLEDs contribute to enhancing resolution, brightness, and color gamut in display technology [11].

In addition, PeLEDs are also promising for near-infrared applications [41], including night vision, telecommunications, and optical switching. In these applications, the emission wavelength within the NIR range (700–2500 nm) plays a crucial role, enabling specific uses such as *in vivo* bio-imaging, biomedical sensing, and optical wireless communications.

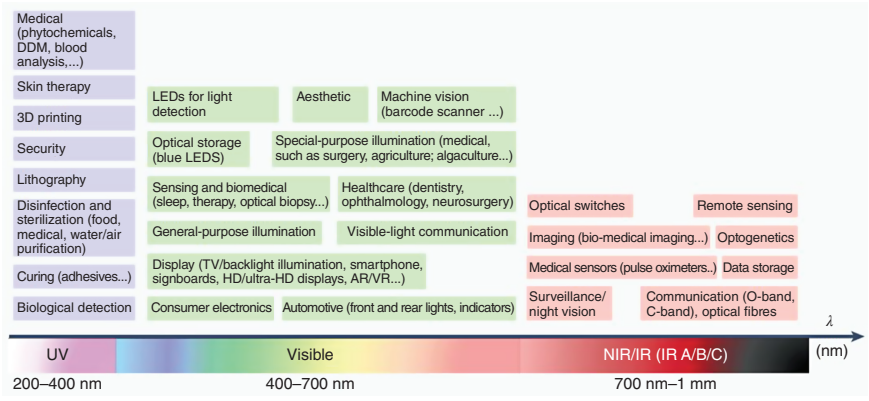

Figure 1.8 Various potential applications of UV-, violet-, visible-, and NIR-emitting PeLEDs. Source: Fakharuddin et al. [11]/Springer Nature.

1.4.1 Photon Generation in Perovskite Materials

The luminescence process in perovskites begins with the formation of an excited-state energy level following photo-excitation or electrical excitation. To achieve efficient photoemission, strong interactions between the injected or photoexcited charges are required, regardless of whether the radiative complex arises from free carriers or excitons [42]. In bulk materials, the large dielectric constants result in relatively low exciton binding energies, and radiative complexes are usually formed by free charge–carrier complexes [43, 44]. The luminescence process in bulk materials is characterized by the radiative recombination of free charge–carrier complexes, which is proportional to the quadratic carrier density. As a result of the large dielectric constants in bulk materials, the exciton binding energies are relatively low, making charge trapping during bimolecular radiative recombination more difficult. The internal bimolecular complexation constants depend on the cross-section and group velocity of the electron–hole exchange interaction. Radiation-free Shockley–Read–Hall (SRH) recombination arises from the trap density of the material, which is not an intrinsic property of the material. The efficiency of this recombination pathway is strongly dependent on the carrier density [42].

The abovementioned recombination pathways can be studied by analyzing the transient spectra of the material. This provides an insight into the rate constants of recombination linked with each pathway [42]. Transient spectra are typically measured at low excitation optical densities, where single-molecule processes are dominant in charge settling and decay, whereas bimolecular processes become more relevant at high excitation optical densities. These spectra can provide valuable information on the recombination constants associated with these different recombination pathways [45].

The interaction among various recombination mechanisms predicts that the highest internal quantum efficiency occurs at carrier densities of 10^{15}–10^{17} cm^{-3},

with a lower non-radiative recombination rate at higher carrier densities. To achieve high luminescence efficiency at carrier densities below $10^{13}\,cm^{-3}$, an extremely low non-radiative recombination rate with a value equivalent to the carrier lifetime at low densities, in the order of microseconds, is required. Alternatively, doping can enhance the emissivity of the perovskite luminescence layer [46]. Obtaining high luminous efficiency at low carrier densities is a challenge for perovskite diodes due to the thinness of the layer and the potential for carriers to cluster and form complexes at localized trapping centers [47]. However, the luminescence of perovskites with strong spatially confined excitons is not significantly affected by carrier density [48, 49].

The charge transport capability of bulk perovskite materials may be affected by perturbations in their crystal structure. To enhance the interaction between charges, the dielectric shielding within the lattice of bulk perovskites can be controlled by utilizing groups with different polarities. This approach enables the enhancement of luminescence efficiency without disrupting charge transport in the bulk crystal structure. However, the interactions between carrier trapping, exciton processes, and their mechanisms are not yet fully understood. The ionic behavior induced by light may alter the bounding potential of the local field and consequently influence the strength of carrier interactions. Further investigations are required to gain a more in-depth understanding of the radiative combination of carriers.

The strong spin–orbit coupling in perovskite materials may lead to Rashba-type energy band splitting, which could impede charge carrier complexation and hinder light transmission in circular photovoltaic effect measurements. Nevertheless, the complexation rates of bimolecules in perovskites remain consistent with those of absorption coefficients and comparable to those of second-order phases with complexation constants in groups III–V, without Rashba effects (a spin–orbit coupling phenomenon observed in solid-state systems, particularly in semiconductor and metal surfaces or interfaces, arising from the interaction between the spin of electrons and their motion in a crystal lattice under the influence of an electric field, leads to the splitting of electronic energy bands and the lifting of spin degeneracy.) Both are approximately on the order of 10^{-10} cm^3 s^{-1} [50]. To address these seemingly contradictory findings, it is crucial to take into account lattice dynamics or carrier localization effects. Additionally, more research is necessary to investigate the dependence of the bimolecular complex constant on carrier temperature and directly analyze the Rashba effect. Furthermore, it is important to examine the dynamical processes that occur after photoexcitation of halide perovskites. Over the past few years, several studies have explored the Rashba effect and its influence on carrier lifetimes in perovskites [51, 52].

As shown in Figure 1.9, the singlet energy level is lower than the triplet energy level due to the combined effect of spin and short-range electron–hole exchange. However, theoretical calculations indicate that significant Rashba coefficients can alter the fine structure of $CsPbX_3$ perovskite nanocrystals, leading to the generation of bright triplet excitons with energies lower than those of the dark monochromatic excitons. The ratio of bright triplet excitons to total excitons can reach as high as 3 : 4, indicating an η_r (radiative efficiency) of the $CsPbX_3$ nanocrystals as high as 0.75.

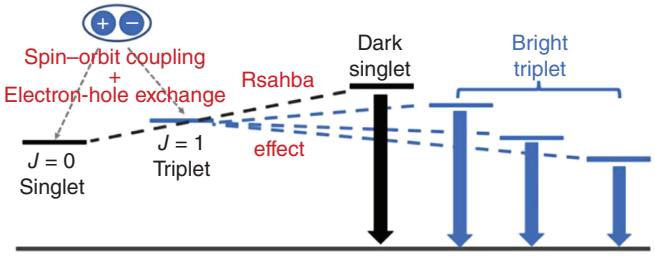

Figure 1.9 The fine structure of excitons in $CsPbX_3$ perovskite nanocrystals considering short-range electron–hole exchange and large Rashba effects [18]. Source: Copyright 2020, Chinese Chemical Society.

These nanocrystals exhibit rapid light emission with decay times on the order of picoseconds (ps) [18].

In recent years, the Rashba effect and its impact on carrier lifetimes in perovskites have been extensively studied. Current research is focused on understanding the underlying causes of the Rashba effect in perovskites, experimental verification of this effect, and its influence on carrier complexes under various environmental conditions [53, 54]. The researcher has also directed their attention toward investigating the Rashba effect in perovskites. However, there have been various viewpoints among researchers regarding the existence of the Rashba effect in perovskites [55]. Some researchers hold the view that the Rashba effect is not a significant issue in perovskites, which is based on arguments that suggest the Rashba effect either does not exist in perovskites or that the luminescence is not thermally activated. However, these seemingly contradictory findings can be reconciled by taking into account the lattice dynamics or carrier localization effects. To arrive at a conclusive understanding, it is essential to measure the dependence of the bimolecular complex constant on carrier temperature and conduct a more direct analysis of the Rashba effect. Additionally, it is necessary to investigate the dynamical processes that occur after photoexcitation of halide perovskites.

1.4.2 Photophysical Processes and Efficiency Calculations of Perovskite Luminescence

Perovskite luminescence involves a series of steps. Initially, under optical and electrical excitation, electrons and holes are generated in the conduction and valence bands. This is followed by a competition between radiative and non-radiative processes, which is influenced by the dimensionality and structure of the perovskite material (Figure 1.10). For instance, in the three-dimensional methylammonium lead iodide ($CH_3NH_3PbI_3$, $MAPbI_3$) perovskite, there is a dephasing time of approximately 220 fs after the initial excitation, during which the ground and excited states are in a superposition state. This dephasing time is three times longer than that observed in GaAs [56]. The dephasing time in $MAPbI_3$ perovskites is not influenced by the number of carriers, indicating that carrier scattering within the measurable

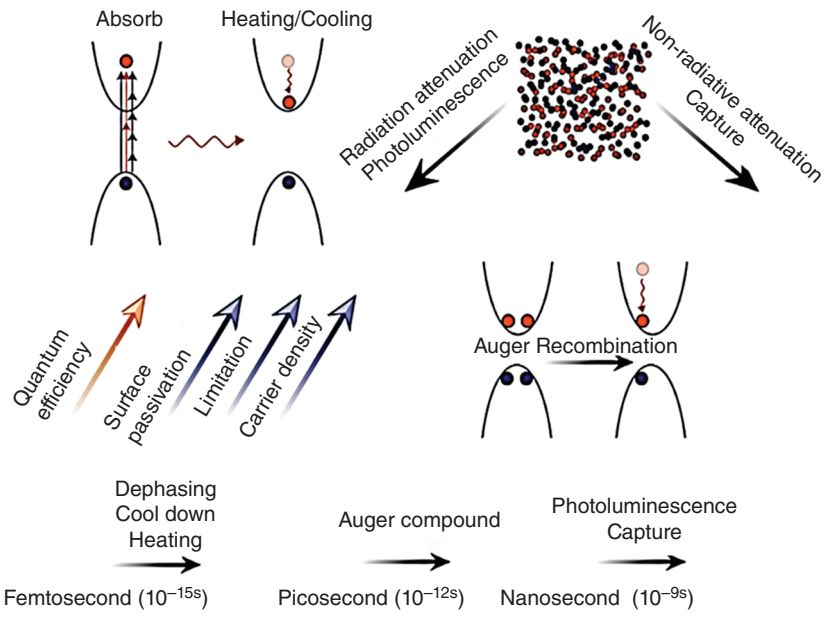

Figure 1.10 Physical processes in perovskite following photoexcitation, with intermittent combinations and non-radiative processes competing with the luminescence process. Source: Quan et al. [9]/John Wiley & Sons.

range is insignificant. However, for quasi-2D I-based perovskites, bulk scattering plays a more substantial role, and the dephasing time decreases with decreasing quantum confinement space [57].

Following dephasing, the excited state undergoes thermal exchange with other particles, such as carriers. In $MAPbI_3$, this process is primarily driven by carrier scattering, leading to thermal exchange times in the order of 10–85 fs [58]. After a duration of over 100 fs, carriers undergo a cooling process. However, under high-density light excitation, this time may be significantly prolonged due to the bottleneck effect of phonons [59–61]. For instance, cooling times of approximately 300 ps have been observed in amidine-based lead iodide ($NH_2CHNH_2PbI_3$, $FAPbI_3$) [55]. In $MAPbI_{3-x}Cl_x$, a decay time of approximately 45 ps was detected, and it stemmed from the thermal exchange process between the organic and inorganic sublattices [62].

At the conclusion of the ultrafast process described earlier, the competition between radiative and non-radiative decay pathways commences. In perovskite materials, non-radiative pathways result from charge trapping. In three-dimensional perovskites, the prevalence of charge trap recombination at low power can significantly limit quantum efficiency. At higher power, radiative recombination becomes more dominant, and close to 100% quantum efficiency can be achieved. This approach can be applied to LEDs. However, their external quantum efficiency (EQE) remains low due to the lack of charge-limited domains.

Through all the above processes, the EQE of the device can be expressed as Eq. (1.3) [11].

$$\mathrm{EQE} = \frac{\text{Photons emitted into free space}}{\text{Charges injected into the emitter film}} = \eta_{\mathrm{inj}} \times \eta_{\mathrm{rad}} \times \eta_{\mathrm{out}} \tag{1.3}$$

Here, η_{out} refers to the outcoupling efficiency, which depends on the optical losses resulting from the mismatched refractive indices between the various device layers, substrate, and air, leading to waveguide and substrate mode effects. The radiative recombination efficiency (η_{rad}) denotes the ratio of the radiatively recombined excitons, whose states allow for optical transitions, to the total excitons generated within the device. The injection efficiency (η_{inj}) describes the number of charge carriers passing the device electrodes that are injected into the perovskite EML.

Researchers have investigated two-dimensional perovskites to achieve high quantum efficiencies at low excitation densities, primarily because of their superior exciton stability at room temperature. However, while nearly 100% quantum efficiency of fluorescence has been achieved at low temperatures [63], the quantum efficiency at room temperature is still very low, which is due to the thermal quenching of the exciton [64]. Furthermore, trapping becomes more significant when the perovskite's dimensionality is reduced from three to two dimensions, as shown in research [65]. Mixed-phase quasi-two-dimensional perovskites demonstrate higher internal and external quantum efficiencies in the near-infrared and visible emission regions [66–68]. The improvement in luminescence efficiency is mainly due to the existence of an energy potential well, which localizes the charge to the lowest energy region, enabling the radiative recombination process to compete with charge trapping. However, for perovskite nanocrystals, surface traps can significantly reduce the quantum efficiency. Therefore, surface passivation has been identified as an effective approach to enhance the luminescence performance [69].

At high excitation power, the elevated carrier concentration and limited rate of radiative recombination can result in exciton annihilation, where excess carriers collide with each other during the diffusion process, leading to a non-radiative recombination process known as intermittent recombination. As the carrier concentration increases, radiative recombination competes with interstitial recombination until a threshold is reached, at which point the excess energy is rapidly lost due to cooling, resulting in a reduction in fluorescence quantum efficiency. The oscillatory complex increases as the exciton binding energy increases, and this effect is particularly pronounced when the dimensionality of the perovskite is reduced from three to two dimensions [70]. Similarly, an increase in the quantum-limited domain leads to a larger blueshift in the luminescence spectrum due to double exciton absorption [71].

As shown in Figure 1.11, metal halide perovskite films typically exhibit a distinct absorption edge in their absorption spectra [73–76], attributed to the phonon-coupling effects within the crystal. The Urbach energy (a parameter used to describe the absorption tail in the optical absorption spectrum of a material. It provides information about the disorder and imperfections in the material's crystal lattice or band structure) of perovskites is typically very low, at around 13 meV, which is comparable to other high-quality semiconductor materials such as GaAs

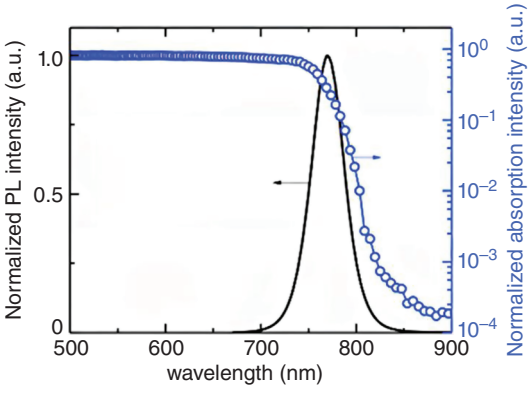

Figure 1.11 Photoluminescence spectrum (left axis) and absorption spectrum (right axis) of the $Cs_{0.06}MA_{0.15}FA_{0.79}Pb(I_{0.85}Br_{0.15})_3$ photothermal reaction deflection spectroscopy test. Source: Stranks et al. [72]/ John Wiley & Sons/CC BY 4.0.

(7.5 meV) and c-Si (9.6 meV) [77, 78]. These properties suggest that metal halide perovskites can maintain low-energy disordered states even at relatively high defect densities and are thus considered to be relatively clean semiconductor materials.

1.4.3 Non-radiative Combination Mechanisms at Surfaces and Interfaces

The EQE of typical perovskite bulk films, such as $MAPbI_3$ or mixed-cation perovskites $(Cs,FA,MA)Pb(I_{0.85}Br_{0.15})_3$, is typically in the range of 1–10% at 1 solar intensity, resulting in a quantum efficiency of less than 50% [45, 77, 78]. This value may increase with increasing carrier density, but it reaches a maximum plateau of less than 100%. This observation is consistent with the non-negligible sub-gap density of states, which in polycrystalline materials has a value of approximately 10^{13}–$10^{15}\,cm^{-3}$ [63, 79], which dominates non-radiative and single-molecule complexes and determines the SRH complex constants. The sub-gap energy states become saturated when the carrier density is lower than the trap density, leading to dominance of radiative and bimolecular recombination processes. However, due to spatial inhomogeneity of trap density, the luminescence can exhibit significant variation between particles when observed on a microscopic scale [80, 81].

Although perovskites exhibit a large number of defects, resulting in many shallow defect states and explaining their defect tolerance, the presence of a large number of deep energy level traps also suggests potential non-radiative losses in such structures [82–85]. One possible origin of such trap states is halide vacancies, which are often found at grain boundaries and surfaces. However, the exact mechanism behind the formation of these trap states is not yet fully understood [77]. These hypotheses have been supported by subsequent studies, which have shown that surface passivation and defect modulation are effective in enhancing luminescence efficiency. For instance, adding KI to the precursors can increase the internal quantum efficiency of thin films up to 95% [77]. KI can serve as a source of iodine to fill vacancies in the halide and also immobilize excess halide with I.

Recent studies have shown that doping can be an effective way to achieve very high efficiencies in perovskite photovoltaic devices [86]. Passivation methods

such as Lewis-based (e.g. pyridine) and trioctylphosphine oxide (TOPO) chemical passivation have been effective in improving the quantum efficiency and luminescence lifetime of perovskites. Post-treatment methods can also extend the carrier lifetime of $MAPbI_3$ films up to 8 μs and increase the internal quantum efficiency up to 90% [87, 88]. Here, it is proposed to combine an electron-donating group with an unoccupied lead site resulting from a halide vacancy [89, 90]. Several studies have demonstrated that exposing thin films and crystals to ambient conditions results in an increase in their internal quantum efficiency and luminescence lifetime, with values exceeding 90%. It is proposed that the presence of photogenerated electrons facilitates the coupling of oxygen in the air to surface vacancies in the halide, leading to the formation of superoxide, which effectively passivates these vacant sites [91].

Nanostructured $CsPbX_3$ exhibits high quantum efficiencies due to the combination of the charge-limited domain and surface passivation. The resulting EQE can exceed 90%. It is worth noting that in nanostructures with dimensions below the emission wavelength, the optical output coupling rate can approach 100%. Layered 2D and quasi-2D structures such as nanoplates can also achieve external quantum efficiencies comparable to those of quantum dots using this approach [92].

While the quantum efficiency and luminescence lifetime of thin films on glass and quartz substrates are important, the performance of the device is greatly impacted by the interfacial contact between the film and the electrode [78, 93]. Interfacial defects resulting from the contact between the layers can lead to non-radiative recombination and affect photon output coupling. In an ideal scenario, the interfacial contact should not reduce the quantum efficiency or carrier lifetime decay, and all combinations should result in radiative recombination, confined to the perovskite luminescent layer. While pure $(Cs,FA,MA)Pb(I_{0.85}Br_{0.15})_3$ films on ITO glass can achieve an EQE of over 20%, the efficiency decreases to 1% in a typical solar cell structure due to interfacial contact between n-type TiO_2 and p-type Spiro-OMeTAD. Therefore, optimizing interfacial contact is crucial for enhancing device performance [77]. Adding a passivation layer to the structure can effectively suppress efficiency losses in the n-type TiO_2 and p-type Spiro-OMeTAD contacts. This results in a photoelectric conversion efficiency of up to 15%. Furthermore, the loss of open circuit voltage due to radiation limitation is significantly reduced from 0.26 V to 0.11 V compared to structures without a passivation layer [77]. Passivation has been found to be a highly effective means of achieving a photoelectric conversion efficiency of 15% and extending the luminescent lifetime in full cells. However, in PeLEDs, TiO_2 and Spiro-OMeTAD have shown very low quantum efficiencies, despite no quenching of the substrate in clean films. This further highlights the presence of interfacial losses [47, 94].

Non-radiative losses at the interface can be reduced by insulating polymer films, such as polystyrene [95] and polyvinylpyrrolidone (PVP) [96]. The incorporation of PVP into the ZnO injection layer and $Cs_{0.87}MA_{0.13}PbBr_3$ film has been shown to enhance fluorescence intensity by a factor of 5 and increase fluorescence quantum efficiency to 55%, resulting in an EQE of 10.4% in device fabrication [96]. Furthermore, interfacial layers consisting of amines such as polyethyleneimine [97] and ethylenediamine [98] have been shown to reduce non-radiative losses and improve

the performance of perovskite-based devices. This enhancement is mainly due to the combination of the N atoms in the amine with the bare lead–halogen framework, which effectively reduces the interfacial defect density. In addition, the use of TOPO can also improve the EQE of the device [89]. Other Lewis-based passivation layers, such as pyridine, have also been shown to have the same effect [99]. However, in these methods, a balance must be found between the increase in the passivation layer and the charge injection potential [19].

The intrinsic bimolecular recombination constant is determined by the cross-section and group velocity of the electron–hole interaction. Together with the non-radiative SRH composite (which depends on the trap density in the material and is an extrinsic property), these composite pathways contribute to the internal quantum efficiency, which is highly reliant on the carrier density in the emission layer (Figure 1.12a). The specific composite constant of a material can generally be determined through transient spectroscopy. Transient luminescence measurements are typically conducted at low excitation densities, where monomolecular processes

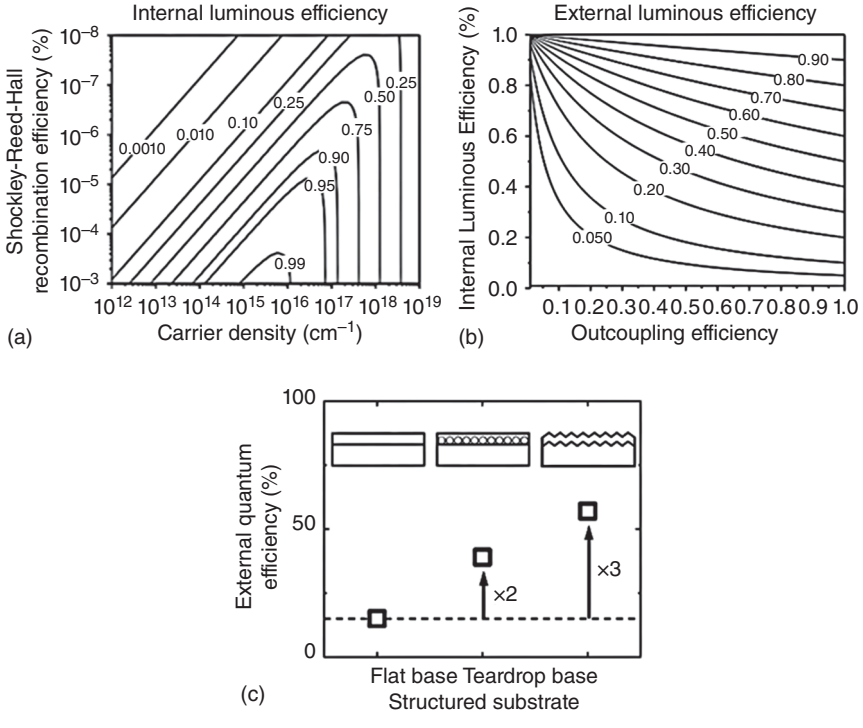

Figure 1.12 (a) Variation of internal quantum luminescence efficiency with carrier density and external Shockley–Read–Hall lifetime calculated using the reported bimolecular composite lifetime and Osher composite lifetime constants; (b) External luminescence quantum efficiency with output coupling efficiency and internal luminescence efficiency taking into account the phonon recycling process; (c) $MAPbBr_3$ film on a microcircuit substrate with external quantum efficiency enhancement. Source: Stranks et al. [72]/John Wiley & Sons/CC BY 4.0.

dominate the charge population decay dynamics. Bimolecular processes are more readily observed at higher excitation densities achievable with amplified laser systems. Moreover, the EQE is strongly influenced by the external coupling efficiency, as a significant portion of the light in the emissive layer can only be internally dissipated due to the distinct refractive indices of the device's various layers. The relationship between internal quantum efficiency, EQE, and external coupling efficiency is illustrated in Figure 1.12b. In general, for planar structures, the EQE limit of the device is approximately 20% (Figure 1.12c). The efficiency can be further improved through the use of mesoporous structures and periodic treatments of the substrate to enhance the external coupling efficiency, consequently enhancing the EQE.

1.5 Factors Influencing the Efficiency of Perovskite Light Emitting Diodes

1.5.1 Device Structure of the Perovskite Light Emitting Diode

The device structures of PeLEDs and organic LEDs are quite similar, both following the traditional "sandwich" structure. As seen in Figure 1.13a,b, there are two types of PeLED device structures based on different preparation processes: the n-i-p inverse structure and the p-i-n formal structure.

In the n-i-p inverse structure, the electron transport layer, perovskite layer, hole transport layer, and electrodes are sequentially prepared on a conductive indium tin oxide glass (ITO glass) substrate. Zinc oxide (ZnO) and tin oxide (SnO_2) are commonly used as electron transport materials, while poly[(9, 9-di-*n*-octylfluorenyl-2, 7-diyl) -alt- (4, 4′-(*N*-[4-*n*-butyl]phenyl)-diphenylamine)] (TFB) is commonly used as the hole transport material. The electrodes are typically made of gold, silver, or aluminum.

In the p-i-n formal structure, the hole transport layer, perovskite layer, electron transport layer, and electrodes are sequentially prepared on an ITO glass substrate. Poly(3,4-ethylenedioxythiophene) (PeDot) and nickel oxide (NiO_x) are commonly used as hole transport materials, while 1, 3, 5-tris(1-phenyl-1*H*-benzimidazol-2-yl)benzene (TPBi) and 1, 3, 5-tris[(3-pyridyl)-3-phenyl]benzene (TmPyPB) are commonly used as electron transport materials. The electrodes are typically made of gold, silver, or aluminum.

Figure 1.13c,d illustrates the transport of electrons and holes in the two device structures. Under external voltage, electrons are generated at the cathode and holes are generated at the anode. They are transported to the perovskite layer via the electron transport layer and hole transport layer, respectively, for radiation compound luminescence.

Figure 1.13e shows a typical architecture of a perovskite LED. The possible active layers constituting a PeLED are labeled on the left, and their contributions to various processes are listed on the right.

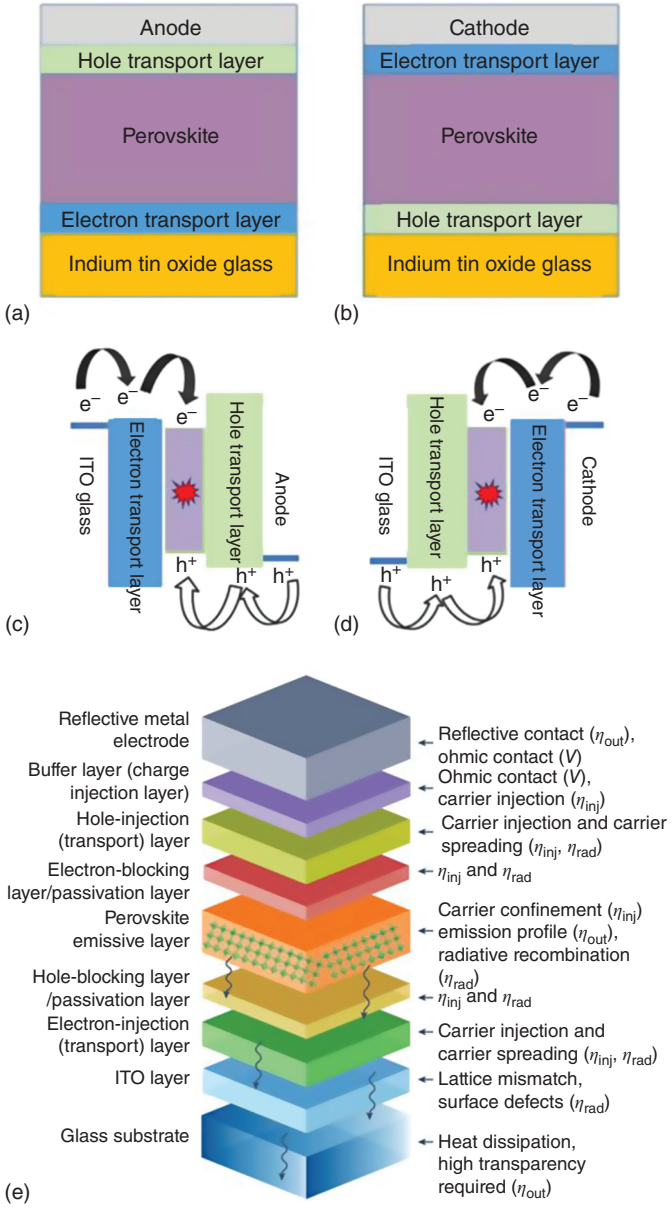

Figure 1.13 Schematic diagram of the structure of a perovskite light-emitting diode device: (a) n-i-p trans structure; (b) p-i-n formal structure; schematic diagram of charge transfer in a perovskite light-emitting diode; (c) trans structure; (d) formal structure; (e) A typical architecture of a perovskite LED. Source: Adapted from Fakharuddin et al. [11].

1.5.2 Physical Parameters of Perovskite Light-Emitting Diodes

Similar to conventional LEDs, the performance of a PeLED can be evaluated based on several physical parameters such as turn-on voltage, brightness or irradiance, peak luminous half-wave width (FWHM), EQE, current efficiency, lumen efficiency, energy conversion efficiency, and stability.

The turn-on voltage is the voltage at which the device starts to operate at a certain level of brightness, typically 1 cd m^{-2} for visible LEDs or when it starts to exhibit an EQE for UV or IR LEDs. The brightness, or irradiance, is the intensity of radiation emitted by the device, measured in cd m^{-2} or W sr^{-1} m^{-2}. The required brightness levels will depend on the intended application of the LED.

The peak-half-peak width of the luminous spectrum represents the purity of the emitted light. A narrower FWHM indicates a purer luminous color, which is desirable for display applications.

EQE is an important measure of light-emitting devices and is defined as the ratio of the number of photons emitted per unit time to the number of electrons injected. It can also be described by the following Eq. (1.4).

$$EQE = f_{\text{balance}} \times f_{\text{e–h}} \times \eta_{\text{radiative}} \times f_{\text{outcoupling}} \tag{1.4}$$

where f_{balance} is the equilibrium charge injection probability (which has a value of 1 when the number of electrons and holes injected is the same), $f_{\text{e-h}}$ is the probability of each carrier pair forming an electron–hole pair or exciton, $\eta_{\text{radiative}}$ is the probability of each electron–hole pair radiating a composite, and $f_{\text{outcoupling}}$ is the optical output coupling rate.

In order to enhance the luminescence efficiency, certain conditions need to be met, including maintaining a balance of electron and hole injection, increasing the chance of electron–hole pair formation, maximizing the ratio of the radiation composite to non-radiation composite, and effectively coupling the generated photons within the luminescent layer to the output. The balance of charge injection in the LED depends on the injection potential of electrons and holes into the perovskite conduction and valence bands, as well as the mobility of electrons and holes, which are limited by the type and properties of the transport layer material. The rate of electron–hole pair formation and combination efficiency can be regarded as the internal quantum efficiency of the material, which is related to material properties such as exciton binding energy and defect density of states. The efficiency of light coupling output mainly depends on the device structure and is subject to the refractive index and shape of the device layers. Typically, the planar structure of an LED limits the light-coupling efficiency to 25%, with most of the photon energy being dissipated in the form of a light waveguide within the device.

Current efficiency is the luminance of the light-emitting device and the ratio of current in cd A^{-1}; lumen efficiency is the ratio of the luminous flux emitted by the device to the electrical power input in lm W^{-1}; and energy conversion efficiency is the ratio of the photon energy emitted by the device to the total energy input.

Stability refers to the operating lifespan of an LED, which is typically measured by the time it takes for the device's brightness or EQE to decay to half of its initial value

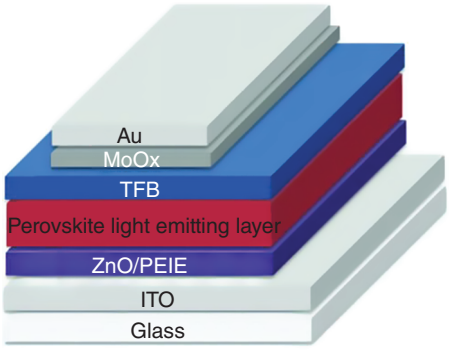

Figure 1.14 Structure diagram of a perovskite light-emitting diode device with ZnO/PEIE as the electron injection layer and TFB as the hole injection layer. Source: Stranks et al. [72]/John Wiley & Sons/CC BY 4.0.

at a constant voltage or current, also known as T50. There are also other measures, such as T90 and T80, which indicate the time taken for the brightness or EQE to decay to 90% and 80% of its initial value, respectively. Devices with better stability are more desirable for commercialization purposes.

Figure 1.14 illustrates the structure of a typical PeLED device. The perovskite light-emitting layer is sandwiched between the electron injection layer ZnO/PEIE and the hole injection layer TFB. When an external electric field is applied, electrons and holes are injected from the electron injection layer and hole injection layer, respectively, and they recombine in the perovskite layer, emitting light. To enhance the efficiency of electron injection, the electron affinity of the electron injection layer can be reduced. For example, doping Mg can form a ZnMgO structure in ZnO, leading to enhanced electron injection efficiency [100, 101]. Alternatively, an additional interface layer, such as polyethyleneimine, can be added between the injection layer and the light-emitting layer to improve electron injection. Similarly, the hole injection barrier can be reduced by doping the hole injection layer with perfluorinated lithium ion salt or by incorporating hole-transporting materials with high HOMO (highest occupied molecular orbital) energy levels, such as 4,4′-bis(9-carbazole) biphenyl, to lower the hole injection barrier [40, 102, 103].

The injection potentials of different layers can be determined by UV photoelectron spectroscopy. However, the energy level structure of perovskites is affected by the substrate work function, which means that UV photoelectron spectroscopy of perovskites requires the film to be deposited on a substrate that closely mimics the device structure. Alternatively, electron absorption spectroscopy can be used to measure the injection barrier in the device [104]. In electron absorption spectroscopy, the effect of the internal electric field on the transmitted light is mainly measured [105]. According to the single-electron Franz–Keldysh–Aspnes low electric field theory, the transmitted light varies with the square of the electric field, which can also be applied to $MAPbI_3$ and other bulk materials [106, 107]. The magnitude of the internal electric field can be measured by modulating the internal electric field with a DC bias. However, the effect of ion shielding has to be taken into account in this process [108].

1.5.3 Device Performance Development of Perovskite Light-Emitting Diodes

In summary, the luminescence and physical properties of perovskite are influenced by several factors. These include the crystal structure of the perovskite, size effects, radiative and non-radiative processes of photons, interface states, and charge injection balance.

In most PeLEDs, the EQE and light output tend to decrease as the current density (J) increases, primarily due to augmented Auger recombination, Joule heating, or imbalanced charge injection. This EQE roll-off phenomenon is also observed in other LED technologies (Figure 1.15b) and typically leads to a 50% decrease in EQE when J ranges from 100 to 1000 mA cm^{-2}. Only a limited number of devices have reported EQE values above 1 A cm^{-2}, and these devices are typically fabricated using pure-phase 2D or mixed-phase 2D/3D perovskite materials (Figure 1.15c). Significantly, PeLEDs with reduced EQE roll-off exhibit low turn-on voltages (V_{ON}), indicating barrier-free charge transport/injection. A low driving voltage can also help alleviate the quantum-confined Stark effect, which is another potential cause for EQE roll-off [11].

Changes in the dimensionality and crystal defects of the perovskite affect the state of the exciton and carrier transport, resulting in a significant change in device performance. In two-dimensional and one-dimensional perovskites, the exciton binding energy is stronger, resulting in a wider color gamut. In contrast, three-dimensional perovskites have a weaker exciton binding energy, leading to a narrower color spectrum. Crystal defects impact the carrier transport capacity, and higher defect densities lead to more exciton capture, resulting in more non-radiative output and reduced device efficiency.

Radiative and non-radiative processes of photons are closely linked to the crystal structure, size effects, exciton binding energy, and trap density, influencing the combination path of excitons. Excitation light density also affects radiation and decay processes. Surface and interface trap states significantly influence non-radiative processes, and surface state modulation can improve device luminous efficiency. Charge injection balance mainly depends on the energy level structure of the material layers and the ideal balance of injection potential at the interface, ensuring both stable device operation and improved EQE.

Although PeLED research started later than that of perovskite solar cells, it has experienced significant development in a short period. In just a few years, the EQE of PeLEDs has increased from less than 0.1% to over 20% [110–114]. To date, the maximum EQEs for near-infrared, red, green, blue, and white light-emitting perovskite diodes have reached 25.5%, 25.8%, 30.84%, 18.65%, and 12.2%, respectively [115–119] (Figure 1.16).

Figure 1.17a presents a comparison of the color gamut of LFMHP-based LEDs, demonstrating that the blue and red components have already fulfilled the requirements of the Rec. 2020 standard, while the green component still requires further improvement. Another critical factor limiting the commercialization of PeLEDs is device lifetime. Figure 1.17b illustrates the promising device stability

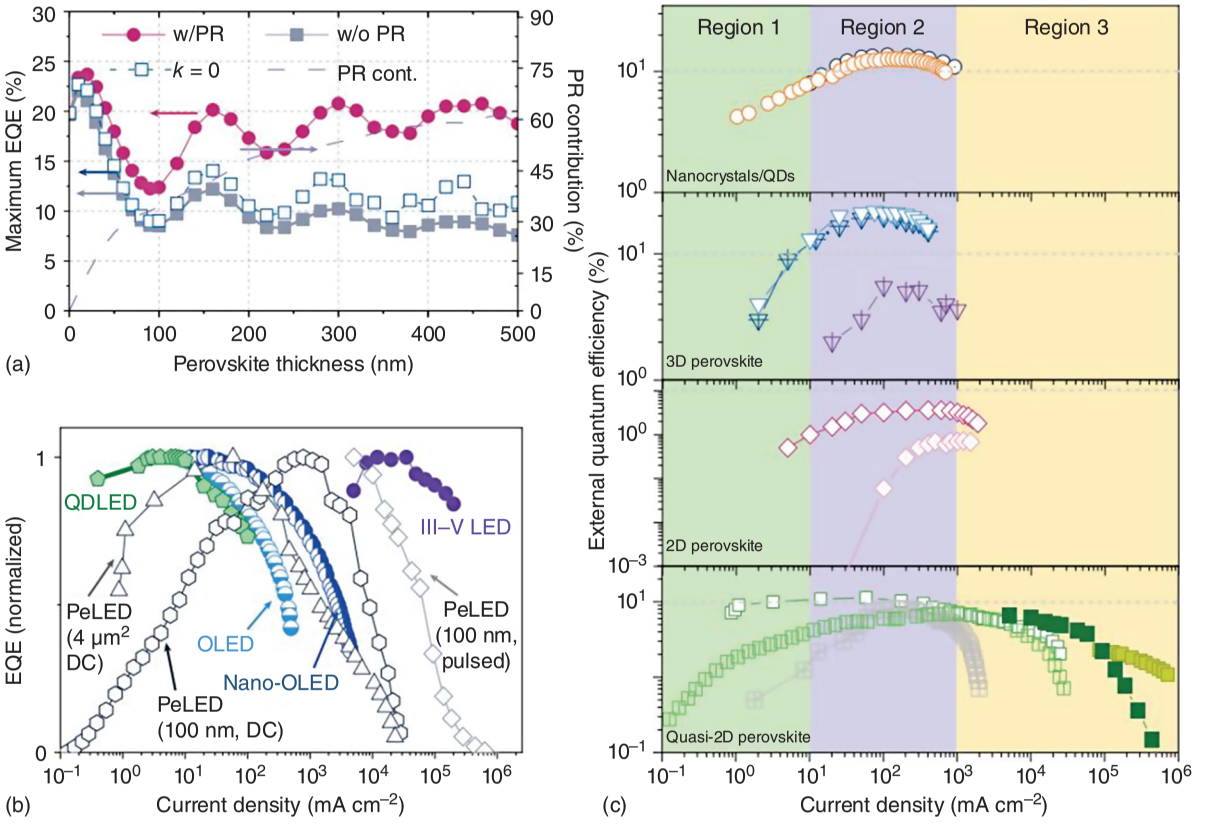

Figure 1.15 Photon-recycling and EQE roll-off in PeLEDs. (a) Calculated EQEs with and without photon recycling (PR; filled red circles and filled gray squares, respectively) and without reabsorption (open navy blue squares), as well as the relative photon recycling contribution (violet dashed lines) for an ideal PeLED (IQE = 100%) with perovskite EMLs of various thickness. *k* indicates the refractive index component connected to the absorption coefficient. Source: Cho et al. [109]/Springer Nature/CC BY 4.0. (b) A comparison of EQE roll-off in various thin-film LEDs (organic LEDs, OLEDs and nano-OLEDs, QDLEDs, and PeLEDs with state-of-the-art crystalline III–V LEDs). DC, direct current. LEDs are biased via steady-state voltage. Source: Fakharuddin et al. [11]/Springer Nature. (c) EQE roll-off trends of some notable PeLEDs reported in the literature employing NCs, 3D, 2D, and 2D/3D EMLs. The plot is divided into three regions based on injection current densities and the type of EML. Source: Fakharuddin et al. [11]/Springer Nature.

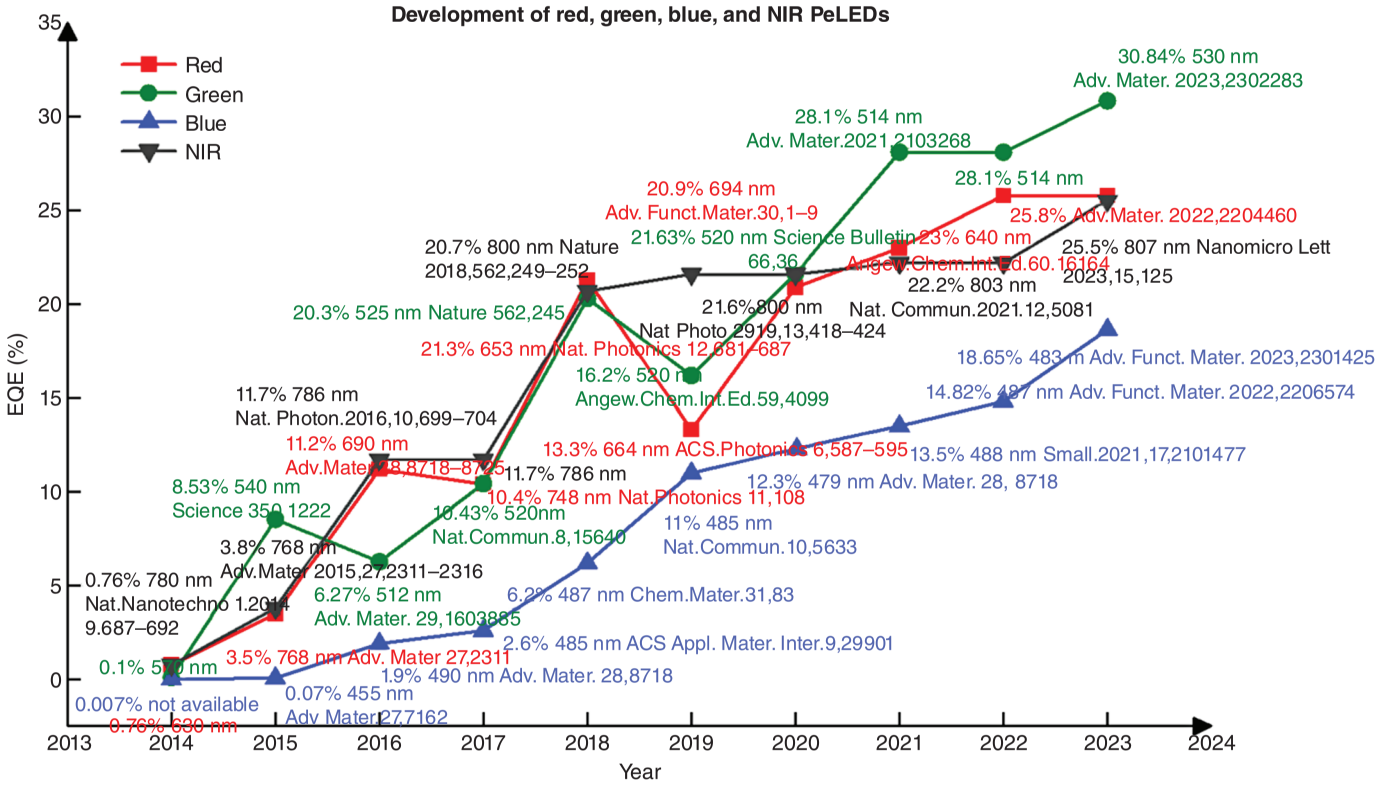

Figure 1.16 The development in EQEs of red, green, blue, and NIR PeLEDs.

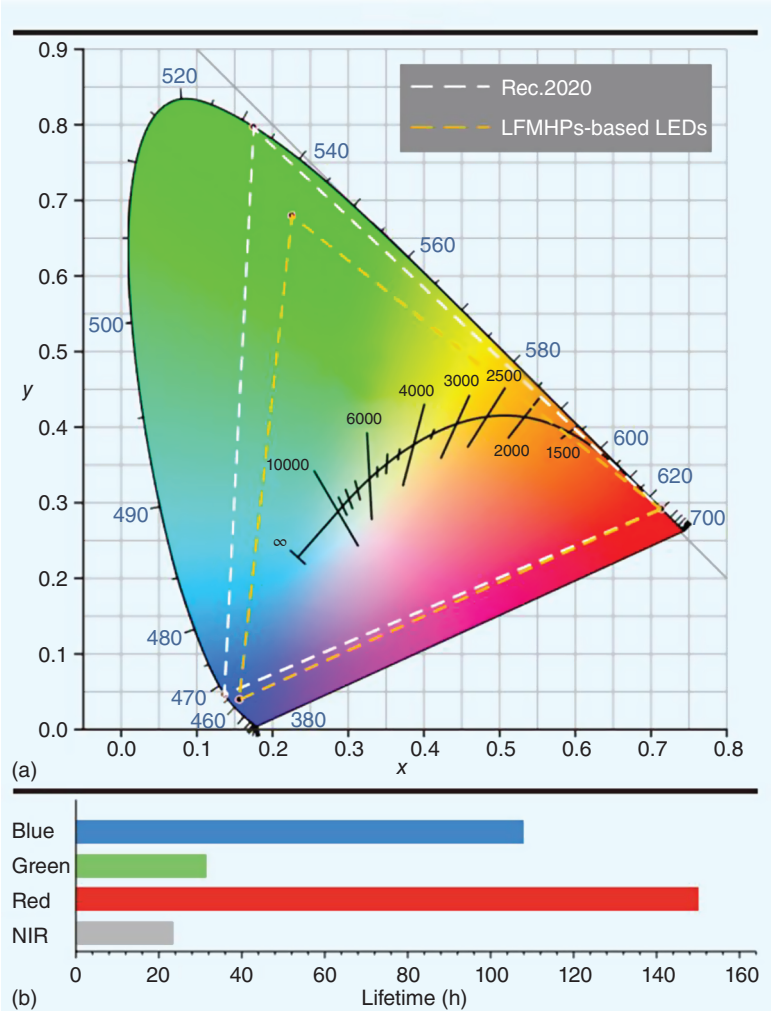

Figure 1.17 Current status of perovskite light-emitting diodes (PeLEDs) based on lead-free metal halide perovskite (LFMHP) emitters. (a) Color gamut coverage of Rec. 2020 and LFMHP-based PeLEDs. (b) Device lifetime of state-of-the-art NIR, red, green, and blue-emitting LFMHP-based PeLEDs. Source: Wang et al. [120]/Innovation Press Co., Limited.

of LFMHP-based LEDs, indicating their potential in overcoming the inherent chemical instability issue found in LHP-based LEDs [120].

1.6 Summary

Perovskite materials are highly sought after for their luminescent properties, including their ability to emit light when excited by an external energy source. This

luminescence is due to the presence of a bandgap in the electronic structure of the material, which allows for the absorption and re-emission of light. This chapter discusses the structure and luminescent properties of perovskite materials, as well as some important physical parameters of PeLEDs and their current development status.

Metal halide perovskites, composed of a lead or tin cation, a halide anion (such as iodide or bromide), and an organic or inorganic A-site cation (such as methylammonium or cesium), are an important class of perovskite materials for optoelectronic applications. These materials exhibit high defect tolerance, which means they can accommodate a high density of defects and impurities without significantly degrading their electronic and optical properties. Metal halide perovskites exhibit a range of luminescent properties, including strong photoluminescence (PL) and electroluminescence (EL) across the visible spectrum. The crystal structure and composition of the material, as well as the presence of defects and impurities, strongly influence their PL and EL properties.

Perovskite LEDs have the potential to operate under ultra-high brightness conditions, allowing for the passage of high currents ($100\,cm^2\ V^{-1}S^{-1}$ or higher) through the diode without causing detrimental processes. This provides an advantage over organic and colloidal quantum dot semiconductors in high-brightness operations. Peak brightness exceeding $10^5\,cd\,m^{-2}$ has been achieved [96], and a recent encouraging aging report using two-dimensional perovskites in LEDs demonstrated no significant degradation in device operation at a current density of $A\,cm^{-2}$ [121].

However, the high-brightness operation of perovskite LEDs is currently hindered by other factors, including the instability of ionic materials under an electric field (ionic migration) [122], imbalanced carrier injection, and non-radiative and Auger recombination losses that occur mainly under low/high injection conditions [123]. These factors may further contribute to the degradation associated with heating.

Perovskite materials also show promise for other applications, such as solar cells, LEDs, lasers, and sensors. Their unique combination of properties, including high defect tolerance, tunable bandgap, and excellent charge transport properties, makes them an attractive candidate for a wide range of optoelectronic applications. Perovskite materials have also been explored for use in sensors, particularly for detecting gases and ions, due to their unique electronic properties, high surface area, and ability to selectively bind to certain molecules.

However, perovskite materials have some challenges that need to be addressed before they can be widely deployed in commercial applications. Their instability in the presence of moisture and oxygen can lead to degradation over time, which is a major obstacle for the development of perovskite-based solar cells. Researchers have made progress in addressing this issue through the development of encapsulation strategies and the use of stable electrode materials, but further work is needed to improve long-term stability. The toxicity of some of the elements used in perovskite materials, particularly lead, is another challenge. While there has been progress in developing lead-free perovskites, many of these materials have lower performance than their lead-based counterparts.

Furthermore, PeLEDs still face challenges in terms of the poor efficiency of blue devices, a decline in EQE under high-brightness conditions, and insufficient device lifespans. The low efficiency of blue PeLEDs is often attributed to halide segregation in mixed Cl–Br perovskite emitters. Some progress has been made through compositional adjustments and the incorporation of bulky organic cations in low-dimensional perovskites. Large organic cations can stiffen the perovskite crystal structure, reducing detrimental electron–phonon interactions and ion migration. However, these cations are typically insulating, resulting in inferior charge transport and reduced device performance. One potential solution is to replace these insulating ligands, commonly alkyl-chained, with conjugated semiconducting ligands, which could potentially alleviate this issue [11].

EQE roll-off and operational stability are significant challenges for PeLEDs, influenced by both intrinsic factors of the perovskite active layer and extrinsic parameters of the device. Ongoing strategies to address these challenges include compositional and dimensional engineering of the perovskite emitter, formation of defect-free emissive layers (EMLs) through passivation techniques, optimization of heterointerfaces to enable barrier-free charge transport and injection, achieving balanced charge injection, operating the devices at low voltages, and reducing the transport resistance in the emissive layer. Given the ionic nature of halide perovskites, the development of specific biasing schemes (e.g. pulsed biasing) may assist in minimizing ion migration and enhancing stability [11].

There is also a need for more research on the potential environmental impact of large-scale perovskite production and deployment, as well as the scalability and reproducibility of perovskite synthesis and device fabrication.

Despite these challenges, perovskite materials hold tremendous potential for a range of applications, and the field is likely to see continued rapid development and progress in the coming years. Advances in perovskite synthesis and device engineering have led to significant improvements in performance, and it is likely that perovskites will continue to be a focus of research and development. Further improvements in performance and stability, as well as the development of new applications and markets for perovskite materials, are expected as continued research and development in this area progresses.

References

1 You, Y.M., Liao, W.Q., Zhao, D. et al. (2017). An organic-inorganic perovskite ferroelectric with large piezoelectric response. *Science* 357: 306–309.

2 Møller, C.K. (1958). Crystal structure and photoconductivity of caesium plumbohalides. *Nature* 182: 1436–1436.

3 Bansal, V., Poddar, P., Ahmad, A. et al. (2006). Room-temperature biosynthesis of ferroelectric barium titanate nanoparticles. *Journal of the American Chemical Society* 128: 11958–11963.

4 Bednorz, J.G. and Müller, K.A. (1986). Possible high Tc superconductivity in the Ba-La-Cu-O system. *Zeitschrift für Physik B Condensed Matter* 64: 189–193.

5 Jin, S., Tiefel, T.H., McCormack, M. et al. (1994). Thousandfold change in resistivity in magnetoresistive La-Ca-Mn-O films. *Science* 264: 413–415.

6 Miao, X., Zhang, L., Wu, L. et al. (2019). Quadruple perovskite ruthenate as a highly efficient catalyst for acidic water oxidation. *Nature Communications* 10: 1–7.

7 Zhao, Y.C., Zhou, W.K., Zhou, X. et al. (2017). Quantification of light-enhanced ionic transport in lead iodide perovskite thin films and its solar cell applications. *Light: Science & Applications* 6: 16243–16243.

8 Mitzi, D.B. (2001). Thin-film deposition of organic-inorganic hybrid materials. *Chemistry of Materials* 13: 3283–3298.

9 Quan, L.N., Garcia de Arquer, F.P., Sabatini, R.P. et al. (2018). Perovskites for light emission. *Advanced Materials* 30: 1801996.

10 Kojima, A., Teshima, K., Shirai, Y. et al. (2009). Organometal halide perovskites as visible-light sensitizers for photovoltaic cells. *Journal of the American Chemical Society* 131: 6050–6051.

11 Fakharuddin, A., Gangishetty, M.K., Abdi-Jalebi, M. et al. (2022). Perovskite light-emitting diodes. *Nature Electronics* 5: 203–216.

12 Kang, J. and Wang, L.W. (2017). High defect tolerance in lead halide perovskite $CsPbBr_3$. *The Journal of Physical Chemistry Letters* 8: 489–493.

13 Yettapu, G.R., Talukdar, D., Sarkar, S. et al. (2016). Terahertz conductivity within colloidal $CsPbBr_3$ perovskite nanocrystals: remarkably high carrier mobilities and large diffusion lengths. *Nano Letters* 16: 4838–4848.

14 Shi, D., Adinolfi, V., Comin, R. et al. (2015). Low trap-state density and long carrier diffusion in organolead trihalide perovskite single crystals. *Science* 347: 519–522.

15 Brandt, R.E., Stevanović, V., Ginley, D.S. et al. (2015). Identifying defect-tolerant semiconductors with high minority-carrier lifetimes: beyond hybrid lead halide perovskites. *MRS Communications* 5: 265–275.

16 Mesquita, I., Andrade, L., and Mendes, A. (2018). Perovskite solar cells: materials, configurations and stability. *Renewable and Sustainable Energy Reviews* 82: 2471–2489.

17 Liu, A., Bi, C., Guo, R. et al. (2021). Electroluminescence principle and performance improvement of metal halide perovskite light-emitting diodes. *Advanced Optical Materials* 9.

18 Zhao, C., Zhang, D., and Qin, C. (2020). Perovskite light-emitting diodes. *CCS Chemistry* 2: 859–869.

19 Cheng, H., Feng, Y., Fu, Y. et al. (2022). Understanding and minimizing non-radiative recombination losses in perovskite light-emitting diodes. *Journal of Materials Chemistry C* 10: 13590–13610.

20 Shi, Z., Li, Y., Zhang, Y. et al. (2017). High-efficiency and air-stable perovskite quantum dots light-emitting diodes with an all-inorganic heterostructure. *Nano letters* 17: 313–321.

21 Han, B., Cai, B., Shan, Q. et al. (2018). Stable, efficient red perovskite light-emitting diodes by (α, δ)-$CsPbI_3$ phase engineering. *Advanced Functional Materials* 28: 1804285.

22 Ban, M., Zou, Y., Rivett, J.P.H. et al. (2018). Solution-processed perovskite light emitting diodes with efficiency exceeding 15% through additive-controlled nanostructure tailoring. *Nature Communications* 9: 1–10.

23 Protesescu, L., Yakunin, S., Kumar, S. et al. (2017). Dismantling the "red wall" of colloidal perovskites: highly luminescent formamidinium and formamidinium-cesium lead iodide nanocrystals. *ACS Nano* 11: 3119–3134.

24 Schweinberger, F.F., Berr, M.J., Doblinger, M. et al. (2013). Cluster size effects in the photocatalytic hydrogen evolution reaction. *Journal of the American Chemical Society* 135: 13262–13265.

25 Dresselhaus (2022). *Optical Properties of Solids*. Oxford University Press.

26 Zhu, X.Y. and Podzorov, V. (2015). Charge carriers in hybrid organic inorganic lead halide perovskites might be protected as large polarons. *The Journal of Physical Chemistry Letters* 6: 4758–4761.

27 Smith, M.D. and Karunadasa, H.I. (2018). White light emission from layered halide perovskites. *Accounts of Chemical Research* 51: 619–627.

28 Tokizaki, T., Makimura, T., Akiyama, H. et al. (1991). Femtosecond cascade-excitation spectroscopy for nonradiative deexcitation and lattice relaxation of the self-trapped exciton in NaCl. *Physical Review Letters* 67: 2701–2704.

29 Zhang, L., Sun, C., He, T. et al. (2021). High-performance quasi-2D perovskite light-emitting diodes: from materials to devices. *Light: Science & Applications* 10: 61.

30 Efros, A.L., Rosen, M., Kuno, M. et al. (1996). Band-edge exciton in quantum dots of semiconductors with a degenerate valence band: dark and bright exciton states. *Physical Review B* 54: 4843–4856.

31 Franceschetti, A., Fu, H., Wang, L.W. et al. (1999). Many-body pseudopotential theory of excitons in InP and CdSe quantum dots. *Physical Review B* 60: 1819–1829.

32 Leung, K., Pokrant, S., and Whaley, K.B. (1998). Exciton fine structure in CdSe nanoclusters. *Physical Review B* 57: 12291–12301.

33 Crooker, S.A., Barrick, T., Hollingsworth, J.A. et al. (2003). Multiple temperature regimes of radiative decay in CdSe nanocrystal quantum dots: intrinsic limits to the dark-exciton lifetime. *Applied Physics Letters* 82: 2793–2795.

34 Labeau, O., Tamarat, P., and Lounis, B. (2003). Temperature dependence of the luminescence lifetime of single CdSe/ZnS quantum dots. *Physical Review Letters* 90: 257404.

35 Donegá, C.M., Bode, M., and Meijerink, M. (2006). Size- and temperature-dependence of exciton lifetimes in CdSe quantum dots. *Physical Review B* 74: 085320.

36 Wang, H., Donegá, C.M., Meijerink, A. et al. (2006). Ultrafast exciton dynamics in CdSe quantum dots studied from bleaching recovery and fluorescence transients. *The Journal of Physical Chemistry B* 110: 733–737.

37 Zhao, Q., Peter, A., Wesley, B.J. et al. (2007). Shape dependence of band-edge exciton fine structure in CdSe nanocrystals. *Nano Letters* 7: 3274–3280.

38 Oron, D., Aharoni, A., Donega, C.M. et al. (2009). Universal role of discrete acoustic phonons in the low-temperature optical emission of colloidal quantum dots. *Physical Review Letters* 102: 177402.

39 Schaller, R.D., Crooker, S.A., Bussian, D.A. et al. (2010). Revealing the exciton fine structure of PbSe nanocrystal quantum dots using optical spectroscopy in high magnetic fields. *Physical Review Letters* 105: 067403.

40 Veldhuis, S.A., Boix, P.P., Yantara, N. et al. (2016). Perovskite materials for light-emitting diodes and lasers. *Advanced Materials* 28: 6804–6834.

41 Vasilopoulou, M., Fakharuddin, A., García de Arquer, F.P. et al. (2021). Advances in solution-processed near-infrared light-emitting diodes. *Nature Photonics* 15: 656–669.

42 Richter, J.M., Abdi-Jalebi, M., Sadhanala, A. et al. (2016). Enhancing photoluminescence yields in lead halide perovskites by photon recycling and light out-coupling. *Nature Communications* 7: 13941.

43 Lin, Q., Armin, A., Nagiri, R.C. et al. (2014). Electro-optics of perovskite solar cells. *Nature Photonics* 9: 106–112.

44 Saba, M., Cadelano, M., Marongiu, D. et al. (2014). Correlated electron-hole plasma in organometal perovskites. *Nature Communications* 5: 5049.

45 Deschler, F., Price, M., Pathak, S. et al. (2014). High photoluminescence efficiency and optically pumped lasing in solution-processed mixed halide perovskite semiconductors. *The Journal of Physical Chemistry Letters* 5: 1421–1426.

46 Wang, H., Zhang, X., Wu, Q. et al. (2019). Trifluoroacetate induced small-grained $CsPbBr_3$ perovskite films result in efficient and stable light-emitting devices. *Nature Communications* 10: 665.

47 Tan, Z.K., Moghaddam, R.S., Lai, M.L. et al. (2014). Bright light-emitting diodes based on organometal halide perovskite. *Nature Nanotechnology* 9: 687–692.

48 Congreve, D.N., Weidman, M.C., Seitz, M. et al. (2017). Tunable light-emitting diodes utilizing quantum-confined layered perovskite emitters. *ACS Photonics* 4: 476–481.

49 Li, G., Tan, Z.K., Di, D. et al. (2015). Efficient light-emitting diodes based on nanocrystalline perovskite in a dielectric polymer matrix. *Nano Letters* 15: 2640–2644.

50 Hutter, E.M., Gelvez-Rueda, M.C., Osherov, A. et al. (2017). Direct-indirect character of the bandgap in methylammonium lead iodide perovskite. *Nature Materials* 16: 115–120.

51 Etienne, T., Mosconi, E., and De Angelis, F. (2016). Dynamical origin of the Rashba effect in organohalide lead perovskites: a key to suppressed carrier recombination in perovskite solar cells? *The Journal of Physical Chemistry Letters* 7: 1638–1645.

52 Davies, C.L., Filip, M.R., Patel, J.B. et al. (2018). Bimolecular recombination in methylammonium lead triiodide perovskite is an inverse absorption process. *Nature Communications* 9: 293.

53 Niesner, D., Wilhelm, M., Levchuk, I. et al. (2016). Giant Rashba splitting in $CH_3NH_3PbBr_3$ organic-inorganic perovskite. *Physical Review Letters* 117: 126401.

54 Isarov, M., Tan, L.Z., Bodnarchuk, M.I. et al. (2017). Rashba effect in a single colloidal $CsPbBr_3$ perovskite nanocrystal detected by magneto-optical measurements. *Nano Letters* 17: 5020–5026.

55 Stroppa, A., Di Sante, D., Barone, P. et al. (2014). Tunable ferroelectric polarization and its interplay with spin-orbit coupling in tin iodide perovskites. *Nature Communications* 5.

56 March, S.A., Riley, D.B., Clegg, C. et al. (2017). Four-wave mixing in perovskite photovoltaic materials reveals long dephasing times and weaker many-body interactions than GaAs. *ACS Photonics* 4: 1515–1521.

57 Elkins, M.H., Pensack, R., Proppe, A.H. et al. (2017). Biexciton resonances reveal exciton localization in stacked perovskite quantum wells. *The Journal of Physical Chemistry Letters* 8: 3895–3901.

58 Richter, J.M., Branchi, F., de Almeida Camargo, F.V. et al. (2017). Ultrafast carrier thermalization in lead iodide perovskite probed with two-dimensional electronic spectroscopy. *Nature Communications* 8: 376.

59 Price, M.B., Butkus, J., Jellicoe, T.C. et al. (2015). Hot-carrier cooling and photoinduced refractive index changes in organic-inorganic lead halide perovskites. *Nature Communications* 6: 8420.

60 Yang, J., Wen, X., Xia, H. et al. (2017). Acoustic-optical phonon up-conversion and hot-phonon bottleneck in lead-halide perovskites. *Nature Communications* 8: 14120.

61 Yang, Y., Ostrowski, D.P., France, R.M. et al. (2015). Observation of a hot-phonon bottleneck in lead-iodide perovskites. *Nature Photonics* 10: 53–59.

62 Chang, A.Y., Cho, Y.J., Chen, K.C. et al. (2016). Slow organic-to-inorganic sub-lattice thermalization in methylammonium lead halide perovskites observed by ultrafast photoluminescence. *Advanced Energy Materials* 6: 1600422.

63 Stranks, S.D., Burlakov, V.M., Leijtens, T. et al. (2014). Recombination kinetics in organic-inorganic perovskites: excitons, free charge, and subgap states. *Physical Review Applied* 2: 034007.

64 Chondroudis, K. and Mitzi, D.B. (1999). Electroluminescence from an organic-inorganic perovskite incorporating a quaterthiophene dye within lead halide perovskite layers. *Chemistry of Materials* 11: 3028–3030.

65 Wu, X., Trinh, M.T., Niesner, D. et al. (2015). Trap states in lead iodide perovskites. *Journal of the American Chemical Society* 137: 2089–2096.

66 Xiao, Z., Kerner, R.A., Zhao, L. et al. (2017). Efficient perovskite light-emitting diodes featuring nanometre-sized crystallites. *Nature Photonics* 11: 108–115.

67 Yuan, M., Quan, L.N., Comin, R. et al. (2016). Perovskite energy funnels for efficient light-emitting diodes. *Nature Nanotechnology* 11: 872–877.

68 Quan, L.N., Zhao, Y., Garcia de Arquer, F.P. et al. (2017). Tailoring the energy landscape in quasi-2D halide perovskites for efficient light emission. *Nano Letters* 17: 3701–3709.

69 Pan, J., Quan, L.N., Zhao, Y. et al. (2016). Highly efficient perovskite-quantum-dot light-emitting diodes by surface engineering. *Advanced Materials* 28: 8718–8725.

70 Milot, R.L., Sutton, R.J., Eperon, G.E. et al. (2016). Charge-carrier dynamics in 2D hybrid metal-halide perovskites. *Nano Letters* 16: 7001–7007.

71 Yang, Y., Yang, M., Li, Z. et al. (2015). Comparison of recombination dynamics in $CH_3NH_3PbBr_3$ and $CH_3NH_3PbI_3$ perovskite films: influence of exciton binding energy. *The Journal of Physical Chemistry Letters* 6: 4688–4692.

72 Stranks, S.D., Hoye, R.L., Di, D. et al. (2019). The physics of light emission in halide perovskite devices. *Advanced Materials* 31: 1803336.

73 Stranks, S.D. and Snaith, H.J. (2015). Metal-halide perovskites for photovoltaic and light-emitting devices. *Nature Nanotechnology* 10: 391–402.

74 Green, M.A., Ho-Baillie, A., and Snaith, H.J. (2014). The emergence of perovskite solar cells. *Nature Photonics* 8: 506–514.

75 De Wolf, S., Holovsky, J., Moon, S.J. et al. (2014). Organometallic halide perovskites: sharp optical absorption edge and its relation to photovoltaic performance. *The Journal of Physical Chemistry Letters* 5: 1035–1039.

76 Sadhanala, A., Deschler, F., Thomas, T.H. et al. (2014). Preparation of single-phase films of $CH_3NH_3Pb(I_{1-x}Br_x)_3$ with sharp optical band edges. *The Journal of Physical Chemistry Letters* 5: 2501–2505.

77 Abdi-Jalebi, M., Andaji-Garmaroudi, Z., Cacovich, S. et al. (2018). Maximizing and stabilizing luminescence from halide perovskites with potassium passivation. *Nature* 555: 497–501.

78 Stranks, S.D. (2017). Nonradiative losses in metal halide perovskites. *ACS Energy Letters* 2: 1515–1525.

79 Wehrenfennig, C., Eperon, G.E., Johnston, M.B. et al. (2014). High charge carrier mobilities and lifetimes in organolead trihalide perovskites. *Advanced Materials* 26: 1584–1589.

80 Draguta, S., Thakur, S., Morozov, Y.V. et al. (2016). Spatially non-uniform trap state densities in solution-processed hybrid perovskite thin films. *The Journal of Physical Chemistry Letters* 7: 715–721.

81 Wu, C., Wu, T., Yang, Y. et al. (2019). Alternative type two-dimensional-three-dimensional lead halide perovskite with inorganic sodium ions as a spacer for high-performance light-emitting diodess. *ACS Nano* 13: 1645–1654.

82 Meng, F., Liu, X., Cai, X. et al. (2019). Incorporation of rubidium cations into blue perovskite quantum dot light-emitting diodes via FABr-modified multi-cation hot-injection method. *Nanoscale* 11: 1295–1303.

83 Ke, Y., Wang, N., Kong, D. et al. (2019). Defect passivation for red perovskite light-emitting diodes with improved brightness and stability. *The Journal of Physical Chemistry Letters* 10: 380–385.

84 Kovalenko, M.V., Protesescu, L., and Bodnarchuk, M.I. (2017). Properties and potential optoelectronic applications of lead halide perovskite nanocrystals. *Science* 358: 745–750.

85 Kirchartz, T., Markvart, T., Rau, U. et al. (2018). Impact of small phonon energies on the charge-carrier lifetimes in metal-halide perovskites. *The Journal of Physical Chemistry Letters* 9: 939–946.

86 Yang, W.S., Park, B.W., Jung, E.H. et al. (2017). Iodide management in formamidinium-lead-halide-based perovskite layers for efficient solar cells. *Science* 356: 1376–1379.

87 Braly, I.L., deQuilettes, D.W., Pazos-Outón, L.M. et al. (2018). Hybrid perovskite films approaching the radiative limit with over 90% photoluminescence quantum efficiency. *Nature Photonics* 12: 355–361.

88 Yang, X., Zhang, X., Deng, J. et al. (2018). Efficient green light-emitting diodes based on quasi-two-dimensional composition and phase engineered perovskite with surface passivation. *Nature Communications* 9: 570.

89 deQuilettes, D.W., Koch, S., Burke, S. et al. (2016). Photoluminescence lifetimes exceeding 8 μs and quantum yields exceeding 30% in hybrid perovskite thin films by ligand passivation. *ACS Energy Letters* 1: 438–444.

90 Sadaf, S.M., Ra, Y.H., Nguyen, H.P.T. et al. (2015). Alternating-current InGaN/GaN tunnel junction nanowire white-light emitting diodes. *Nano Letters* 15: 6696–6701.

91 Brenes, R., Eames, C., Bulovic, V. et al. (2018). The impact of atmosphere on the local luminescence properties of metal halide perovskite grains. *Advanced Materials* 30: 1706208.

92 Weidman, M.C., Seitz, M., Stranks, S.D. et al. (2016). Highly tunable colloidal perovskite nanoplatelets through variable cation, metal, and halide composition. *ACS Nano* 10: 7830–7839.

93 Tvingstedt, K., Malinkiewicz, O., Baumann, A. et al. (2014). Radiative efficiency of lead iodide based perovskite solar cells. *Scientific Reports* 4: 6071.

94 Chen, C., Gao, L., Gao, W. et al. (1927). Circularly polarized light detection using chiral hybrid perovskite. *Nature Communications* 2019: 10.

95 Wolff, C.M., Zu, F., Paulke, A. et al. (2017). Reduced interface-mediated recombination for high open-circuit voltages in $CH_3NH_3PbI_3$ solar cells. *Advanced Materials* 29: 1700159.

96 Zhang, L., Yang, X., Jiang, Q. et al. (2017). Ultra-bright and highly efficient inorganic based perovskite light-emitting diodes. *Nature Communications* 8: 15640.

97 Wang, J., Wang, N., Jin, Y. et al. (2015). Interfacial control toward efficient and low-voltage perovskite light-emitting diodes. *Advanced Materials* 27: 2311–2316.

98 Lee, S., Park, J.H., Lee, B.R. et al. (2017). Amine-based passivating materials for enhanced optical properties and performance of organic-inorganic perovskites in light-emitting diodes. *The Journal of Physical Chemistry Letters* 8: 1784–1792.

99 Wu, C.Y., Wang, Z., Liang, L. et al. (2019). Graphene-assisted growth of patterned perovskite films for sensitive light detector and optical image sensor application. *Small* 15: 1900730.

100 Hoye, R.L., Chua, M.R., Musselman, K.P. et al. (2015). Enhanced performance in fluorene-free organometal halide perovskite light-emitting diodes using tunable, low electron affinity oxide electron injectors. *Advanced Materials* 27: 1414–1419.

101 Hoye, R.L., Munoz-Rojas, D., Musselman, K.P. et al. (2015). Synthesis and modeling of uniform complex metal oxides by close-proximity atmospheric pressure chemical vapor deposition. *ACS Applied Materials & Interfaces* 7: 10684–10694.

102 Kim, Y.H., Cho, H., Heo, J.H. et al. (2015). Multicolored organic/inorganic hybrid perovskite light-emitting diodes. *Advanced Materials* 27: 1248–1254.

103 Kim, Y.H., Cho, H., and Lee, T.W. (2016). Metal halide perovskite light emitters. *PNAS* 113: 11694–11702.

104 Hoye, R.L.Z., Schulz, P., Schelhas, L.T. et al. (2017). Perovskite-inspired photovoltaic materials: toward best practices in materials characterization and calculations. *Chemistry of Materials* 29: 1964–1988.

105 Brown, T.M., Kim, J.S., Friend, R.H. et al. (1999). Built-in field electroabsorption spectroscopy of polymer light-emitting diodes incorporating a doped poly(3, 4-ethylene-dioxythiophene) hole injection layer. *Applied Physics Letters* 75: 1679–1681.

106 Ziffer, M.E., Mohammed, J.C., and Ginger, D.S. (2016). Electroabsorption spectroscopy measurements of the exciton binding energy, electron-hole reduced effective mass, and band gap in the perovskite $CH_3NH_3PbI_3$. *ACS Photonics* 3: 1060–1068.

107 Amerling, E., Baniya, S., Lafalce, E. et al. (2017). Electroabsorption spectroscopy studies of $(C_4H_9NH_3)_2PbI_4$ organic-inorganic hybrid perovskite multiple quantum wells. *The Journal of Physical Chemistry Letters* 8: 4557–4564.

108 Campbell, I.H., Hagler, T.W., Smith, D.L. et al. (1900). Direct measurement of conjugated polymer electronic excitation energies using metal/polymer/metal structures. *Physical Review Letters* 1996: 76.

109 Cho, C., Zhao, B., Tainter, G.D. et al. (2020). The role of photon recycling in perovskite light-emitting diodes. *Nature Communications* 11: 611.

110 Song, J., Li, J., Li, X. et al. (2015). Quantum dot light-emitting diodes based on inorganic perovskite cesium lead halides ($CsPbX_3$). *Advanced Materials* 27: 7162–7167.

111 Lu, M., Zhang, X., Zhang, Y. et al. (2018). Simultaneous strontium doping and chlorine surface passivation improve luminescence intensity and stability of $CsPbI_3$ nanocrystals enabling efficient light-emitting devices. *Advanced Materials* 30: 1804691.

112 Song, J., Fang, T., Li, J. et al. (2018). Organic-inorganic hybrid passivation enables perovskite QLEDs with an EQE of 16.48%. *Advanced Materials* 30: 1805409.

113 Chiba, T., Hayashi, Y., Ebe, H. et al. (2018). Anion-exchange red perovskite quantum dots with ammonium iodine salts for highly efficient light-emitting devices. *Nature Photonics* 12: 681–687.

114 Hou, S., Gangishetty, M.K., Quan, Q. et al. (2018). Efficient blue and white perovskite light-emitting diodes via manganese doping. *Joule* 2: 2421–2433.

115 Li, J., Duan, C., Zhang, Q. et al. (2023). Self-generated buried submicrocavities for high-performance near-infrared perovskite light-emitting diode. *Nano-Micro Letters* 15: 125.

116 Chen, Z., Li, Z., Chen, Z. et al. (2021). Utilization of trapped optical modes for white perovskite light-emitting diodes with efficiency over 12%. *Joule* 5: 456–466.

117 Bai, W., Xuan, T., Zhao, H. et al. (2023). Perovskite light-emitting diodes with an external quantum efficiency exceeding 30%. *Advanced Materials* 2302283.

118 Zhou, W., Shen, Y., Cao, L.X. et al. (2023). Manipulating ionic behavior with bifunctional additives for efficient sky-blue perovskite light-emitting diodes. *Advanced Functional Materials* 33: 2301425.

119 Jiang, J., Chu, Z., Yin, Z. et al. (2022). Red perovskite light-emitting diodes with efficiency exceeding 25% realized by co-spacer cations. *Advanced Materials* 34: 2204460.

120 Wang, Z., Zheng, S., Teng, Q. et al. (2023). Opportunity of lead-free metal halide perovskites for electroluminescence. *The Innovation Materials* 1: 100015.

121 Tsai, H., Nie, W., Blancon, J.C. et al. (2018). Stable light-emitting diodes using phase-pure Ruddlesden–Popper layered perovskites. *Advanced Materials* 30: 1704217.

122 Yuan, Y. and Huang, J. (2016). Ion migration in organometal trihalide perovskite and its impact on photovoltaic efficiency and stability. *Accounts of Chemical Research* 49: 286–293.

123 Zou, W., Li, R., Zhang, S. et al. (2018). Minimising efficiency roll-off in high-brightness perovskite light-emitting diodes. *Nature Communications* 9: 608.